



RESEARCH LETTER

10.1002/2017GL073717

Key Points:

- The 2016 Kaikoura earthquake produced tsunami signals that indicate sizeable seafloor deformation in addition to onshore surface ruptures
- Iterative modeling of teleseismic P and SH waves and regional tide and wave gauge recordings indicates two regions of seafloor deformation
- Tsunami excitation involved oblique thrusting on the southern Hikurangi megathrust and offshore extension of transpressional faults

Supporting Information:

- Supporting Information S1
- Movie S1

Correspondence to:

K. F. Cheung,
cheung@hawaii.edu

Citation:

Bai, Y., T. Lay, K. F. Cheung, and L. Ye (2017), Two regions of seafloor deformation generated the tsunami for the 13 November 2016, Kaikoura, New Zealand earthquake, *Geophys. Res. Lett.*, *44*, 6597–6606, doi:10.1002/2017GL073717.

Received 3 APR 2017

Accepted 5 JUN 2017

Accepted article online 12 JUN 2017

Published online 3 JUL 2017

Two regions of seafloor deformation generated the tsunami for the 13 November 2016, Kaikoura, New Zealand earthquake

Yefei Bai¹ , Thorne Lay² , Kwok Fai Cheung¹ , and Lingling Ye³ 

¹Department of Ocean and Resources Engineering, University of Hawaii at Manoa, Honolulu, Hawaii, USA, ²Department of Earth and Planetary Sciences, University of California Santa Cruz, Santa Cruz, California, USA, ³Seismological Laboratory, California Institute of Technology, Pasadena, California, USA

Abstract The 13 November 2016 Kaikoura, New Zealand, M_w 7.8 earthquake ruptured multiple crustal faults in the transpressional Marlborough and North Canterbury tectonic domains of northeastern South Island. The Hikurangi trench and underthrust Pacific slab terminate in the region south of Kaikoura, as the subduction zone transitions to the Alpine fault strike-slip regime. It is difficult to establish whether any coseismic slip occurred on the megathrust from on-land observations. The rupture generated a tsunami well recorded at tide gauges along the eastern coasts and in Chatham Islands, including a ~4 m crest-to-trough signal at Kaikoura where coastal uplift was about 1 m, and at multiple gauges in Wellington Harbor. Iterative modeling of teleseismic body waves and the regional water-level recordings establishes that two regions of seafloor motion produced the tsunami, including an M_w ~7.6 rupture on the megathrust below Kaikoura and comparable size transpressional crustal faulting extending offshore near Cook Strait.

1. Introduction

The Pacific-Australian plate boundary transitions from the Hikurangi subduction zone along North Island of New Zealand to transform faulting along the Alpine Fault in western South Island (Figure 1a). The transition involves distributed transpressive faulting in the Marlborough and North Canterbury tectonic domains [e.g., *Litchfield et al.*, 2014] along with termination of the Hikurangi Trough at the southern edge of the underthrust Pacific slab immediately south of Kaikoura, South Island [e.g., *Furlong*, 2007; *Furlong and Kamp*, 2009]. The underthrust Pacific slab extends beneath the Marlborough Fault Zone; the ~20° dipping megathrust is about 20 km deep below the coastline of northeastern-most South Island [*Williams et al.*, 2013]. Complex transpressional faulting with multiple discrete blocks in the upper plate can account for most of the observed surface deformation produced by the ~38 mm/yr of highly oblique convergence between the Pacific and Australian plates [e.g., *Wallace et al.*, 2007, 2012]. However, beneath southern North Island, geodetic measures of slip-deficit indicate that the shallow megathrust is locked [e.g., *Wallace et al.*, 2009, 2012]. Some megathrust slip deficit is detected beneath Cook Strait and the Canterbury region, but it is less well defined than to the north. A seismic gap at least 200 km long extends along the megathrust to the vicinity of the 9 August 1904 event near 40.5°S [*Hogben*, 1904; *Nishenko and McCann*, 1981].

The M_w 7.8 Kaikoura earthquake struck the northeastern coastal margin of South Island on 13 November 2016 (Figure 2a). The hypocenter was at 42.737°S, 173.054°E and a depth of 15.1 km, with origin time 11:02:56 UTC [*USGS-NEIC*: <https://earthquake.usgs.gov/earthquakes/eventpage/us1000778i#executive>]. The long-period Global CMT [<http://www.globalcmt.org/CMTsearch.html>] and USGS W-phase moment tensors both have M_w 7.8 and similar oblique thrusting focal mechanisms with significant nondouble couple components and large centroid time delays of about 57 s. Observations of surface faulting include a sequence of ~12 faults extending northeastward to the Kekerengu Fault, which has localized horizontal displacements of at least 9 m, and then offshore on the Needles Fault [*Litchfield et al.*, 2016; *Bradley et al.*, 2017; *Hamling et al.*, 2017; *Kääb et al.*, 2017]. The last major earthquake in the region was on 16 October 1848, when a magnitude ~7.5 event ruptured ~100 km of the Awatere Fault [*Mason and Little*, 2006], which parallels the 2016 rupture zone to the northwest.

The 2016 rupture generated a tsunami observed at tide and wave gauges around the coasts of South and North Islands as well as in Chatham Islands. The Kaikoura tide gauge recorded a tsunami with ~4 m height (crest-to-trough) along with 0.9–1.0 m static uplift of the coast. Excitation of tsunami requires sizeable

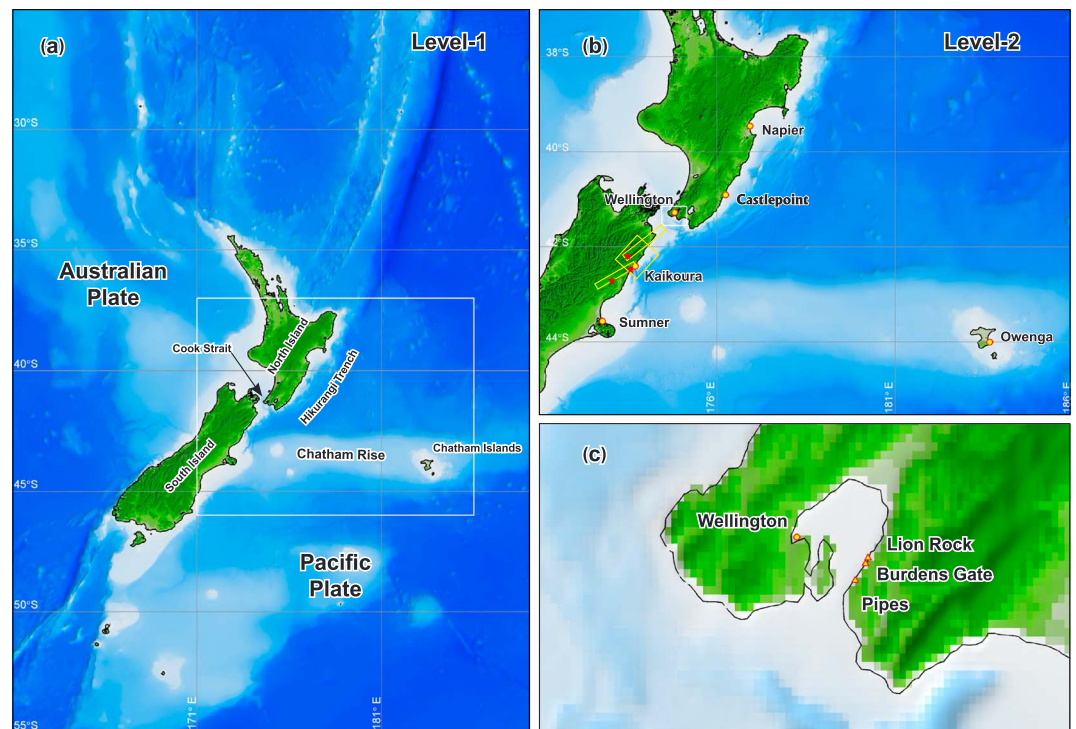


Figure 1. Computational grids and location maps. (a) Level 1 grid at 2 arcmin resolution. White rectangle delineates level 2 grid covering coastlines with distinct tsunami records. (b) Level 2 grid at 30 arcsec resolution. Yellow rectangles denote simplified fault geometries, red stars indicate the respective epicenters, and white rectangle outlines an area for close-up view. (c) Close-up view near Wellington Harbor. Yellow circles and triangles denote tide and wave gauge locations.

seafloor deformation, and it is not immediately clear that the observed surface ruptures can account for the size and timing of the tsunami. We use teleseismic P and SH waves as well as regional water-level observations to explore onshore and offshore faulting with simplified fault geometries and determine the source region for the tsunami. The goal is to evaluate whether slip on the megathrust contributed to the tsunami, as this bears upon the open question of the slip deficit and seismic potential of the southern Hikurangi megathrust.

2. Faulting Representation and Tsunami Model

Preliminary investigations of geodetic, seismic, and field observations indicate very complex faulting with many short segments having variable orientations along the 2016 Kaikoura rupture. Most of the local observations involve predominantly right-lateral slip on steeply dipping faults with modest uplift, but there are some cross-faults with notable local uplift [e.g., *Hamling et al., 2017; Käbb et al., 2017*]. Teleseismic observations indicate that the seismic radiation is relatively weak for the first 60 s of the rupture, followed by a 20 s interval of very strong moment rate. Far-field inversions indicate that the interval of large moment-rate involves significant thrust faulting coincident with shallow strike-slip faulting [e.g., USGS-NEIC finite-fault solution: <https://earthquake.usgs.gov/earthquakes/eventpage/us1000778i#finite-fault>; *Duputel and Rivera, 2017; Hollingsworth et al., 2017*]. The largest aftershock is an M_w 6.5 event 30 min after the mainshock (42.321°S, 173.669°E, 11:32:06 UTC) with a northwest dipping thrust-fault solution [USGS-NEIC]. We adopt a simplified finite-faulting representation (Figure 2a), which comprises two upper crustal faults trending along the rupture zone with geometries consistent with the largest surface displacements and aftershock concentrations as well as an offshore fault representing the megathrust extending from the Hikurangi Trough beneath the coast. We invert broadband teleseismic signals to partition slip onto the three faults for computation of tsunami excitation and iteratively adjust kinematic parameters of the rupture and fault dimensions to self-consistently balance the seismic moment contributions and any offshore faulting required to match the recorded tsunami signals.

We use 86 P wave ground displacements and 47 SH wave ground velocities from global stations filtered between 0.005 and 0.9 Hz in a least-squares finite-fault inversion for the three faults with fixed rupture

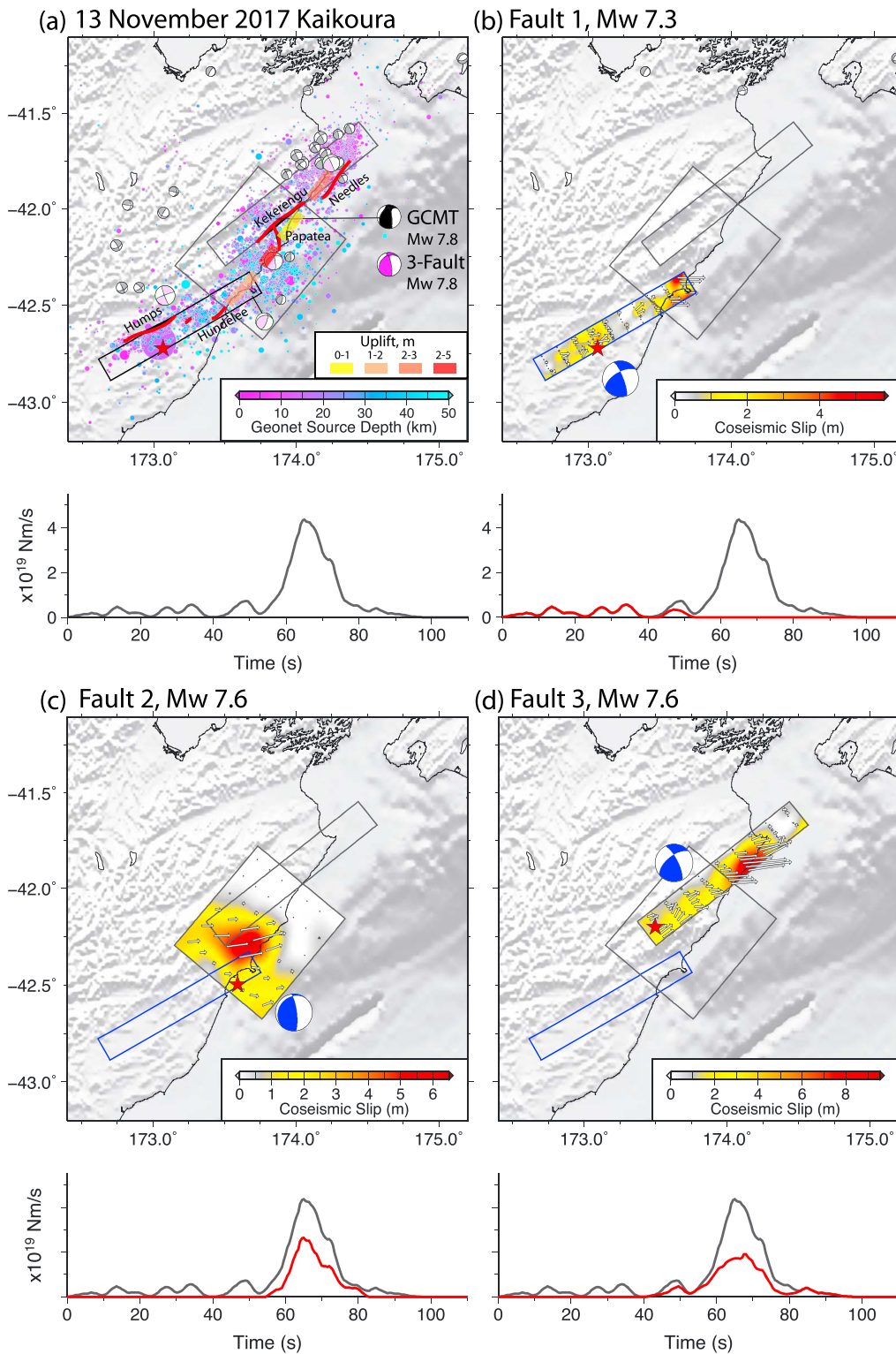


Figure 2. Maps of northeastern South Island, New Zealand showing the preferred rupture model for the 2016 Kaikoura earthquake. (a) Locations of three fault grids (black rectangles) superimposed on aftershock seismicity; circles are scaled with magnitude from the GNS catalogue (<http://info.geonet.org.nz/display/appdata/Earthquake+Catalogue>). The black focal mechanism is the GCMT solution for the mainshock, and the magenta solution is the moment tensor for the three-fault model. Other focal mechanisms are GCMT solutions for prior activity (gray) and aftershocks (color coded by source depth). Locations of surface ruptures are denoted by heavy red lines with associated named faults. Uplift ranges are compiled from <http://info.geonet.org.nz/x/p4A5AQ>. (b) Fault 1 illustrated by slip color scale and vectors with M_w 7.3. (c) Fault 2 with M_w 7.6. (d) Fault 3 with M_w 7.6. Red star indicates the hypocenter, and blue focal mechanism represents the average of each fault. The moment rate function for each fault is shown in red relative to the moment rate function for the total (black).

velocities [e.g., Hartzell and Heaton, 1983]. The fault geometries are specified based on the local surface rupture reports and mapped faults (Figure 2a). The first fault has a strike of 240° with dip of 60° , generally representing the Humps Fault Zone and Hundalee Fault. The second fault has a strike of 220° with a dip of 20° , representing the megathrust that terminates south of Kaikoura and is at a depth of 20 km below the coast. The third fault strikes 232° with a dip of 60° and represents the quasi-continuous sequence of the Jordan Thrust, Kekerengu Fault, and offshore Needles Fault, which appear to have had variable amounts of surface rupture. The teleseismic data cannot resolve small changes in strike and dip along each segment, but we do allow for variable rake on the fault to accommodate transpressional motion. Teleseismic inversions were run with variable rupture velocity from 1.4 to 3.5 km/s, fault dimensions within the aftershock regions, and onset for the second and third segments between 20 to 58 s after the origin time. Resulting models with low residual waveform power were then used to compute tsunami signals, which further guided constraints on the overall model parameters, as successfully done in previous studies [e.g., Lay et al., 2011; Yamazaki et al., 2011b, 2013; Bai et al., 2014; Gusman et al., 2015; Heidarzadeh et al., 2016].

The nonhydrostatic code NEOWAVE facilitates forward modeling of the tsunami from a given fault-slip model [Yamazaki et al., 2009, 2011a]. The shock-capturing finite-difference scheme includes a vertical velocity term in the nonlinear shallow-water equations to account for weakly dispersive waves. The vertical velocity term also describes the time history of seafloor vertical motions from the half-space solution of Okada [1985] and the horizontal displacement on a slope as suggested by Tanioka and Satake [1996]. Modeling of tsunami generation from kinematic seafloor deformation is essential in reproducing recorded signals in the near field [Li et al., 2016]. We model the tsunami with two levels of nested computational grids derived from the 250 m resolution New Zealand Regional Bathymetry. Figures 1a and 1b shows the grid layout and locations of tide and wave gauges considered in this study. The level 1 grid at 2 arcmin (~ 3600 m) resolution covers the shelves and basins around New Zealand to capture resonance modes with periods up to ~ 100 min [Bai et al., 2015]. The level 2 grid provides higher resolution of 30 arcsec (~ 900 m) along coastlines with tsunami measurements. The time steps are 1 and 0.2 s for the level 1 and 2 grids to minimize numerical dissipation and ensure model stability. The selected gauges were well positioned with clear records of the tsunami around the source. In particular, the Kaikoura tide gauge is within the overlapping rupture zones of Faults 1 and 2. There are three wave gauges near the entrance and one tide gauge in the ship basin of Wellington Harbor directly across from Fault 3 (Figure 2c).

3. Kaikoura Rupture and Tsunami Models

We have performed a total of 28 iterations guided by tsunami modeling. Figure 2 shows the preferred three-fault solution accounting for 86% of the observed teleseismic waveform power (see Figures S1 and S2 in the supporting information for details of the slip distributions and comparisons of the observed and predicted P and SH waveforms). For all subfaults within the three segments, the source time functions are parameterized with six symmetric 3 s rise-time triangles, giving possible subfault durations of up to 21 s. Fault 1 initiates at 3 km depth at 42.724°S , 173.065°E on a grid with seven subfaults 4 km wide along dip and 10 subfaults 10 km long along strike. The average rake is 164° , and the seismic moment is 1.07×10^{20} N m (M_w 7.3). The slip is patchy with concentrations near the hypocenter on the Humps fault and near the coast on the Hundalee Fault. The rupture velocity is 2.0 km/s, and rupture continues for about 50 s with mainly strike-slip motion. The megathrust fault begins to rupture 55 s after the origin at 19.2 km deep at 42.498°S , 173.592°E , with rupture spreading northeastward at 3.5 km/s. This fault has seven subfaults along dip with 10 km width and six along strike with 12.5 km length. The average rake is 136° , and the seismic moment is 2.95×10^{20} N m (M_w 7.6). This represents highly oblique slip on the megathrust nearly parallel to the plate convergence direction. Slip of up to 6 m occurs on a patch extending about 36 km beneath the coast north of the Kaikoura peninsula, with modest slip extending updip, only partway to the trench. The third fault begins to rupture 37 s after the origin time, at a hypocenter 15 km deep at 42.200°S , 173.497°E . This rupture extends northeast at 2.5 km/s along the Kekerengu Fault to the coast and then offshore, roughly along the Needles Fault. The fault has seven subfaults 5 km wide along dip and nine subfaults 12.5 km long along strike. The average rake is 159° , and the seismic moment is 3.22×10^{20} N m (M_w 7.6). A large 9 m slip patch is found in the region corresponding to the Kekerengu Fault, consistent with surface rupture observations. The overall faulting has a seismic moment of 7.25×10^{20} N m (M_w 7.8).

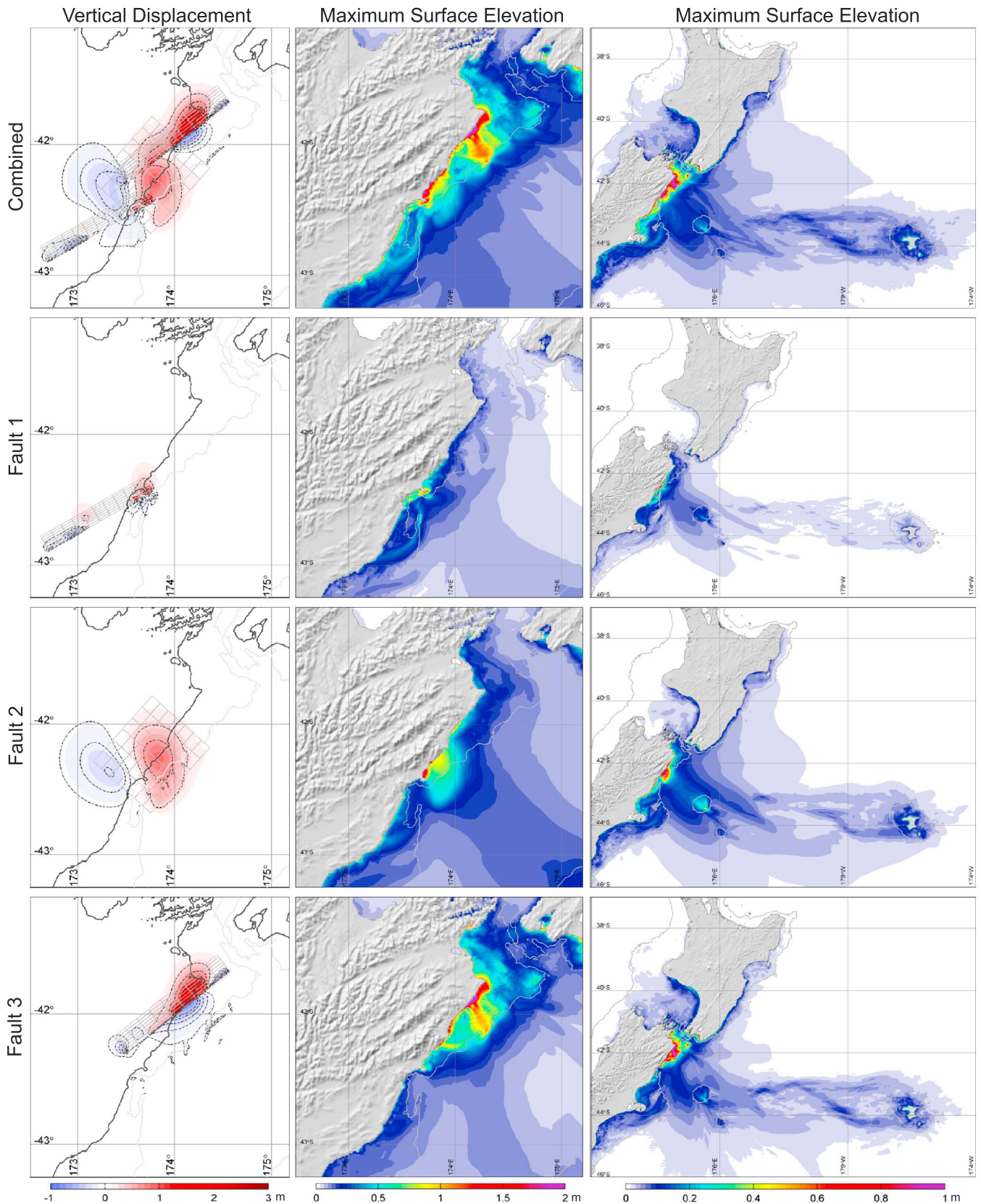


Figure 3. Seafloor vertical displacement and maximum sea-surface elevation from the preferred three-fault model. Gray lines denote the 200 m depth contour delineating the approximate extent of the shelf. Black dash lines are contours of subsidence and uplift at 0.1 and 0.3 m intervals.

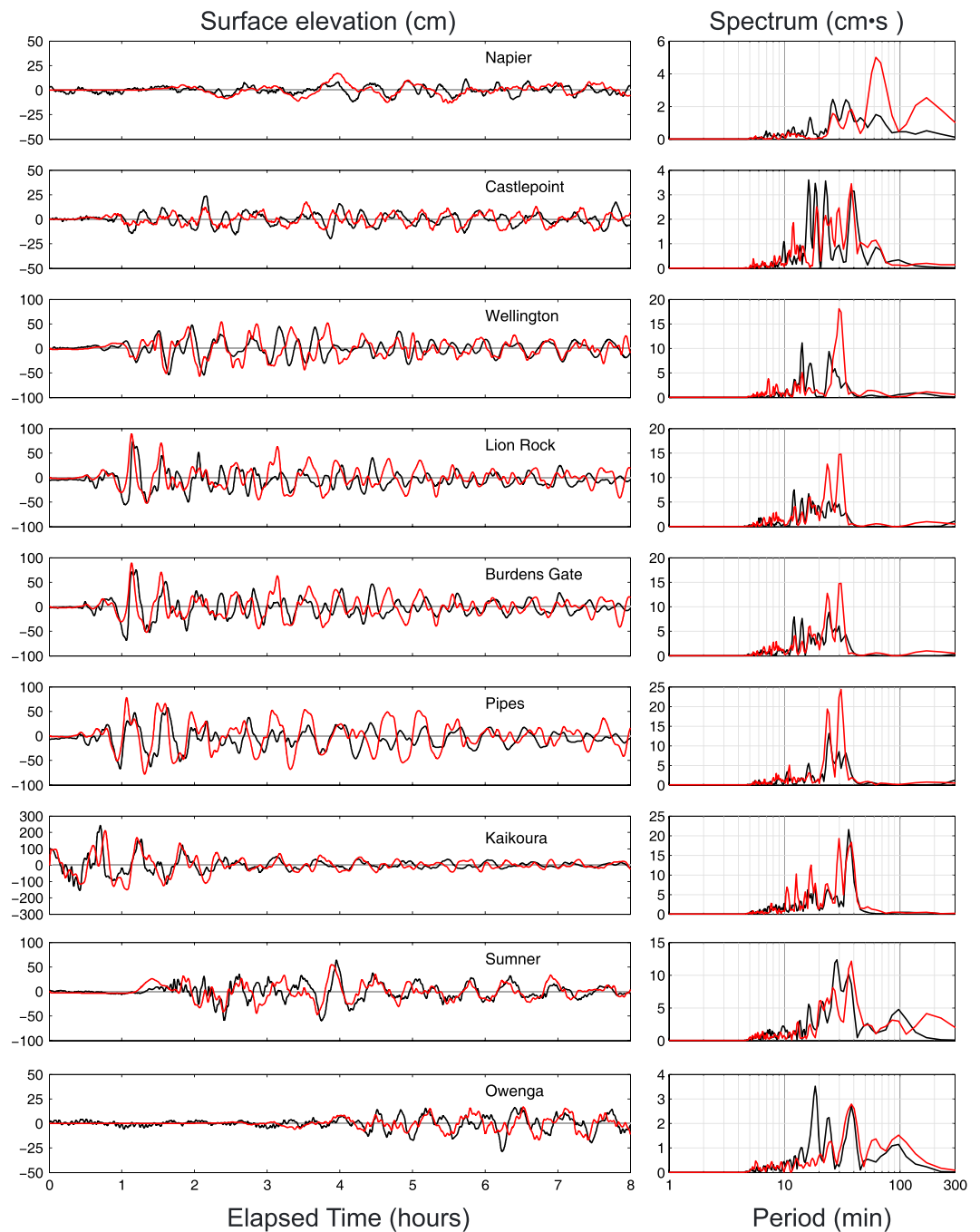
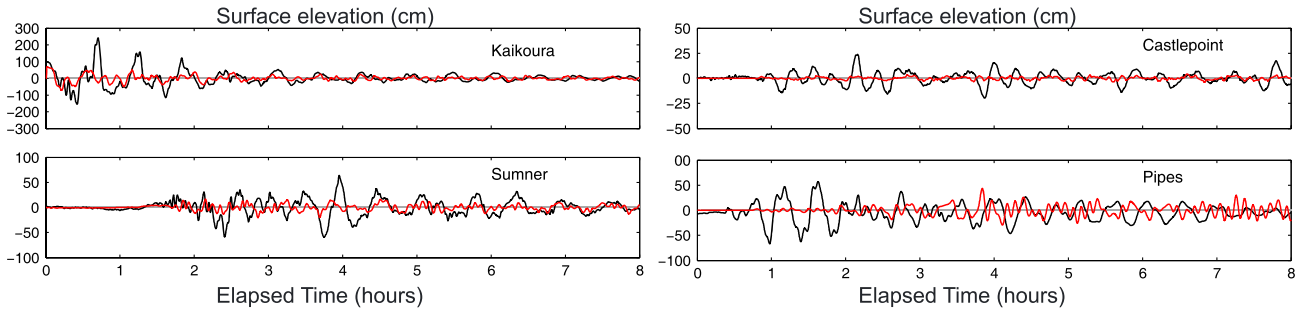


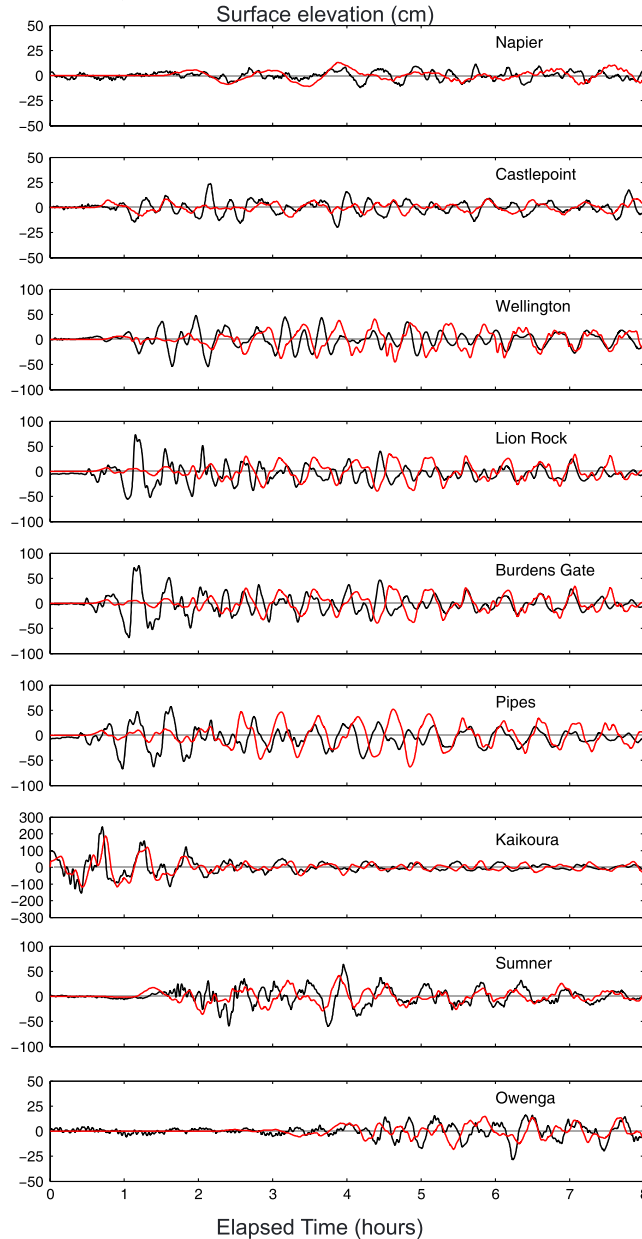
Figure 4. Comparison of tide and wave gauge records (black lines) with computed waveforms and spectra (red lines) from the preferred three-fault model.

The forward tsunami modeling provides strong constraints on the specific timing, fault dimensions, and rupture velocities for the preferred model, and in particular, the amount and extent of slip for Fault 2. Figure 3 shows the seafloor vertical displacement and the near- and far-field sea-surface elevations. The crustal deformation is complex with overlapping uplift and subsidence from the three faults. The tsunami excitations from horizontal displacement are minor as most of the deformation occurs over the shelf. The combined from Faults 1 and 2 is ~1 m at the Kaikoura tide gauge and up to ~1.5 m immediately offshore, and the tsunami has most significant impact along the shores to the northeast. The shelf is discontinuous south of Kaikoura restricting longshore propagation of the tsunami, while Chatham Rise functions as a

(a) Fault 1, Mw 7.3



(b) Fault 2, Mw 7.6



(c) Fault 3, Mw 7.6

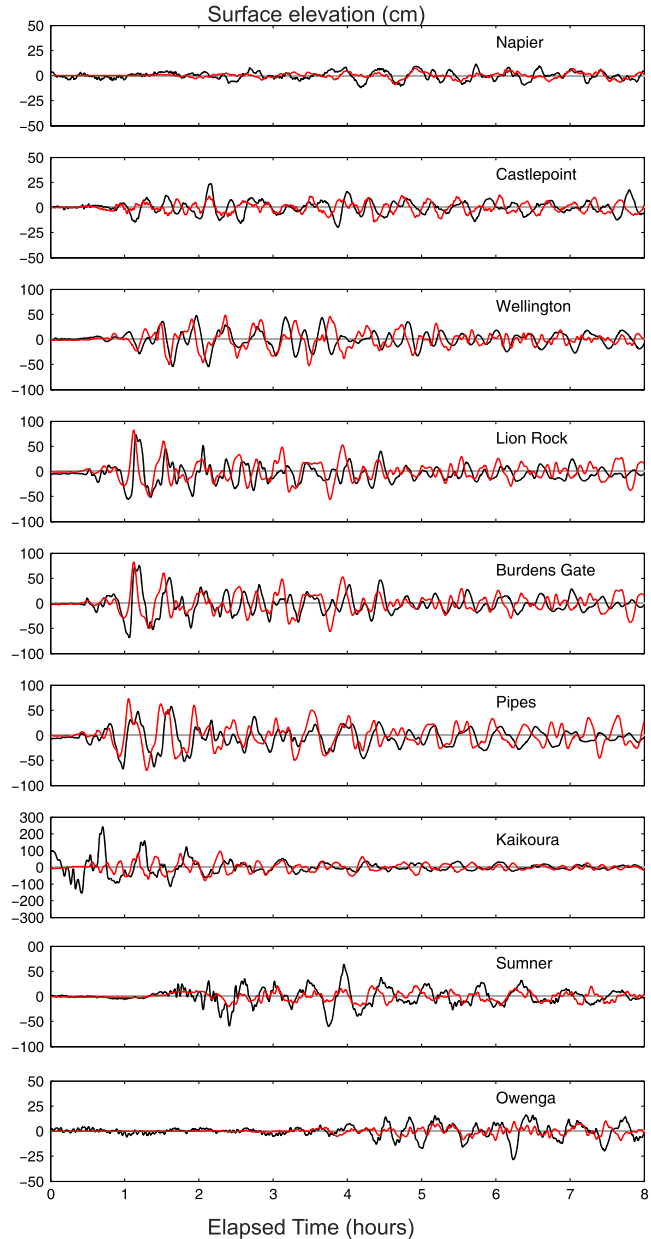


Figure 5. Comparison of tide and wave gauge records (black lines) with computed waveforms (red lines) from separate faults of the preferred model. (a) Fault 1. (b) Fault 2. (c) Fault 3. Due to nonlinearity near the coast, superposition of the waveforms computed for the separate faults does not fully reproduce the results of the complete model in Figure 4.

waveguide for the energy to the east. The individual faults have distinct seafloor deformation contributing to the tsunami. Fault 1 produces concentrated uplift and localized tsunami impact over the shelf at Kaikoura. The largest uplift of 0.9 m from Fault 2 occurs at the shore 20 km northeast of Kaikoura. The uplift region extends beyond the shelf resulting in significant onshore shoaling of the tsunami waves to over 2 m elevation. Fault 3 produces up to 3 m of uplift and 2.5 m of sea-surface rise over the shelf at the northeast corner of South Island. The resulting tsunami waves dominate Cook Strait extending into Wellington Harbor with a distinct oscillation pattern. Both Faults 2 and 3 result in notable wave action on the leeward side of Chatham Islands, where the tide gauge is located.

Figure 4 compares the recorded and computed waveforms and spectra (see Animation M1 in the supporting information to aid interpretation of the results). The uplift near Kaikoura resulted in a vertical datum shift, which manifests as a step decrease of the recorded water surface elevation. We removed the artifact through readjustment of the shifted datum using the mean sea levels computed from the tide gauge records before and after the earthquake. The resulting time series shows an initial sea-surface elevation of 0.95 m due to the seafloor uplift followed by drawdown of the water and arrival of tsunami waves. NEOWAVE reproduces these complex near-field processes at the shore even with relatively low resolution of 30 arcsec in the computation. The good agreement maintains at the gauges in Wellington Harbor to the north and at Sumner to the south. The spectral components of the 8 h time series are reasonably reproduced between 5 to 100 min periods at these near-field locations. The minor time shifts are related to the precise slip placement, which must be reconciled within the three-fault model of this very complex earthquake. The tsunami propagates as edge waves along the shore to reach Castlepoint and Napier and to wrap around Chatham Islands to the tide gauge at Owenga. The computed tsunami matches the overall wave amplitude and dominant spectral components at these locations, but cannot fully reproduce the waveform and phase due to accumulation of errors from the low resolution of the shores.

The observed tsunami is a result of the complex seafloor deformation from the multiple earthquake ruptures. Figure 5 shows contributions from the three faults to the waveforms at the tide and wave gauges (see Animation M1 to aid interpretation). Fault 1 contributes primarily to the initial sea-surface rise at Kaikoura. The concentrated initial pulse, when modeled by itself, produces small-amplitude short-period oscillations that are also seen at nearby locations such as Sumner, Wellington Harbor, and Castlepoint. The mega thrust fault component (Fault 2) also plays a role in the initial sea-surface rise at Kaikoura and accounts for the drawdown prior to arrival of the ~4 m high tsunami wave from the main pulse. Small-amplitude waves generated by the offshore portion of the pulse reach the entrance of Wellington Harbor within ~0.5 h, but the main component over the shelf does not arrive until ~2 h afterward. The narrow harbor entrance amplifies the initial arrivals from Fault 3, which is located across Cook Strait. At tide gauges further from the source, Faults 2 and 3 contribute to the long- and short-period signals related to the size of the rupture region. The far-field signals are useful in confirming the overall wave amplitude and to a certain extent in differentiating the fault contributions in the iterative modeling process.

4. Discussion and Conclusions

The fault model presented here produces tsunami waves by seafloor motions in two distinct regions along the northeast South Island coast as shown in Figure 3. The segment representing the Humps Fault Zone and Hundalee Fault and the megathrust component produce coastal uplift of up to 1 m along Kaikoura extending about 40 km to the northeast. There is then a region with insignificant ground displacement followed by a mix of offshore subsidence and nearshore uplift as the third fault crosses the coast, transitioning from the Kekerengu to the Needles faults. This is generally consistent with the observed pattern of uplift summarized in Figure 2a, although our model does not reproduce the localized 2–5 m uplift associated with the Papatea pop-up structure. Small adjustments in fault orientation and dip might be achieved in more detailed modeling, but the general pattern of seafloor motion of our model is sufficient to match the tsunami waveforms at Kaikoura and in Wellington Harbor adjacent to the source.

We infer that a significant component of the seismic radiation for the 2016 Kaikoura earthquake was released from a shallow dipping fault beneath Kaikoura, which is likely the southernmost portion of the Hikurangi megathrust. The large region of uplift extending offshore is necessary to account for the observed tsunami height of ~4 m. Duputel and Rivera [2017] produce a four point-source model, which has a southern

strike-slip faulting event with M_w 7.2, an M_w 7.4 oblique thrust below the Hope Fault, and then near-coincident M_w 7.6 thrust faulting northeast of Kaikoura and M_w 7.6 strike-slip faulting near the Kekerengu fault. Our three-fault finite-source model is very compatible, and both models give overall moment tensors consistent with the long-period GCMT and W-phase solutions. The USGS-NEIC finite fault solution uses four fault segments and also finds deep oblique thrusting on a megathrust segment that dips 35° below the coast. Deep oblique thrusting on a megathrust is strongly indicated by all of the teleseismic solutions, although there are trade-offs in slip for the simultaneously rupturing megathrust and crustal faults.

Coincident rupture of upper plates and megathrust faults in the region appears to have happened previously. The last great earthquake to strike southern North Island was the 1855 Wairarapa earthquake, with estimated magnitudes of 8.0–8.4 [e.g., *Grapes and Downes*, 1997]. This event produced large surface rupture along the Wairarapa fault, regional uplift of the southwest of North Island, and tsunami runup of 9.1 m east of Wellington [De Lange and Healy, 1986; Darby and Beanland, 1992]. Dislocation modeling of the regional uplift indicates that slip occurred on the deeper part of the underlying plate boundary at depths of about 25 km [Darby and Beanland, 1992; Beavan and Darby, 2005], but does not extend updip to the trench, similar to the 2016 event. Involvement of the megathrust could help account for the observed 1855 tsunami excitation.

Shallow coupling of the Hikurangi megathrust is uncertain. Magnitude ~ 7 events struck offshore of Gisborne in March and May of 1947, producing runup heights of 10 m and 6 m, respectively [De Lange and Healy, 1986; Bell *et al.*, 2014]. The large tsunami and low shaking of both events have been interpreted as the result of tsunami earthquakes [defined by Kanamori, 1972], possibly influenced by local seamounts on the subduction interface in a region where the dominant failure mode is in slow slip events. The 2 February 1931 Hawkes Bay $M \sim 7.8$ earthquake produced the largest reported tsunami runup in New Zealand of 15.3 m [De Lange and Healy, 1986]. This appears to have ruptured the upper plate, Napier reverse dextral fault, and likely a splay fault from the megathrust [Hull, 1990; Kelsey *et al.*, 1998]. It is unclear whether the faults in the Marlborough region have listric connection to the megathrust of similar nature. It appears that the southern Hikurangi megathrust could participate in future large ruptures.

Acknowledgments

The IRIS DMS data center (<http://www.iris.edu/hq/>) was used to access the seismic data from Global Seismic Network and Federation of Digital Seismic Network stations. The New Zealand Regional Bathymetry and tide gauge data were downloaded from the National Institute of Water and Atmospheric Research (<https://www.niwa.co.nz/our-science/oceans/bathymetry>) and Land Information New Zealand (<http://www.linz.govt.nz/sea/tides/sea-level-data/sea-level-data-downloads>), respectively. This data analysis made use of GMT, SAC, and Matlab software. We would like to thank Ian Hamling (GNS Science) for his initial local rupture models, Florian Monetti (MetOcean Solutions) for post-processed data from the three wave gauges in Wellington Harbor, and Mohammad Heidarzadeh (Brunel University) and an anonymous reviewer for their comments on this paper. NOAA provided support through grant NA15NWS4670025 to Kwok Fai Cheung and NSF through grant EAR1245717 to Thorne Lay. SOEST contribution 10016.

References

- Bai, Y., K. F. Cheung, Y. Yamazaki, T. Lay, and L. Ye (2014), Tsunami surges around the Hawaiian Islands from the 1 April 2014 North Chile M_w 8.1 earthquake, *Geophys. Res. Lett.*, *41*, 8512–8521, doi:10.1002/2014GL061686.
- Bai, Y., Y. Yamazaki, and K. F. Cheung (2015), Interconnection of multi-scale standing waves across the Pacific Basin from the 2011 Tohoku tsunami, *Ocean Model.*, *92*, 183–197.
- Beavan, R. J., and D. J. Darby (2005), Fault slip in the 1855 Wairarapa earthquake based on new and reassessed vertical motion observations: Did slip occur on the subduction interface? in *The 1855 Wairarapa Earthquake Symposium: 150 Years of Thinking About Magnitude 8+ Earthquakes and Seismic Hazard in New Zealand: 8–10 September 2005: Proceedings Volume*, edited by J. Townend, R. M. Langridge, and A. Jones, pp. 31–41, Greater Wellington Reg. Council, Wellington.
- Bell, R., C. Holden, W. Power, X. Wang, and G. Downes (2014), Hikurangi margin tsunami earthquake generated by slow seismic rupture over a subducted seamount, *Earth Planet. Sci. Lett.*, *397*, 1–9.
- Bradley, B. A., H. N. T. Razafindrakoto, and V. Polak (2017), Ground-motion observations from the 14 November 2016 M_w 7.8 Kaikoura, New Zealand earthquake and insights from broadband simulations, *Seismol. Res. Lett.*, *88*(3), 1–17.
- Darby, D. J., and S. Beanland (1992), Possible source models for the 1855 Wairarapa earthquake, New Zealand, *J. Geophys. Res.*, *97*, 12,375–12,389, doi:10.1029/92JB00567.
- De Lange, W. P., and T. R. Healy (1986), New Zealand tsunamis 1840–1982, *N. Z. J. Geol. Geophys.*, *29*, 115–134.
- Duputel, Z., and L. Rivera (2017), Long-period analysis of the 2016 Kaikoura earthquake, *Phys. Earth Planet. Inter.*, *265*, 62–66, doi:10.1016/j.pepi.2017.02.004.
- Furlong, K. P. (2007), Locating the deep extent of the plate boundary along the Alpine Fault zone, New Zealand: Implications for patterns of exhumation in the Southern Alps, *Geol. Soc. Am. Spec. Pap.*, *434*, 1–14.
- Furlong, K. P., and P. J. J. Kamp (2009), The lithospheric geodynamics of plate boundary transpression in New Zealand: Initiating and emplacing subduction along the Hikurangi margin, and the tectonic evolution of the Alpine Fault system, *Tectonophysics*, *474*, 449–462.
- Grapes, R., and G. Downes (1997), The 1855 Wairarapa, New Zealand, earthquake: Analysis of historical data, *Bull. N.Z. Soc. Earthquake Eng.*, *30*(4), 271–368.
- Gusman, A. R., S. Murotani, K. Satake, M. Heidarzadeh, E. Gunawan, S. Watada, and B. Schurr (2015), Fault slip distribution of the 2014 Iquique, Chile, earthquake estimated from ocean-wide tsunami waveforms and GPS data, *Geophys. Res. Lett.*, *42*, 1053–1060, doi:10.1002/2014GL062604.
- Hamling, I. J., *et al.* (2017), Complex multifault rupture during the 2016 M_w 7.8 Kaikoura earthquake, New Zealand, *Science*, *356*, eaam7194, doi:10.1126/science.aam7194.
- Hartzell, S. H., and T. H. Heaton (1983), Inversion of strong ground motion and teleseismic waveform data for the fault rupture history of the 1979 Imperial Valley, California, earthquake, *Bull. Seismol. Soc. Am.*, *73*(6A), 1553–1583.
- Heidarzadeh, M., T. Harada, K. Satake, T. Ishibe, and A. R. Gusman (2016), Comparative study of two tsunamigenic earthquakes in the Solomon Islands: 2015 M_w 7.0 normal-fault and 2013 Santa Cruz M_w 8.0 megathrust earthquakes, *Geophys. Res. Lett.*, *43*, 4340–4349, doi:10.1002/2016GL068601.

- Hogben, G. (1904), Notes on the East Coast earthquake of 9th August 1904, *Trans. New Zealand Inst.*, *37*, 421–424.
- Hollingsworth, J., L. Ye, and J.-P. Avouac (2017), Dynamically triggered slip on a splay fault in the M_w 7.8, 2016 Kaikoura (New Zealand) earthquake, *Geophys. Res. Lett.*, *44*, 3517–3525, doi:10.1002/2016GL072228.
- Hull, A. G. (1990), Tectonics of the 1931 Hawke's Bay earthquake, *New Zeal. J. Geol. Geophys.*, *33*, 309–320.
- Käb, A., B. Altena, and J. Mascaro (2017), Coseismic displacements of the 14 November 2016 M_w 7.8 Kaikoura, New Zealand, earthquake using an optical cubesat constellation, *Nat. Hazards Earth Syst. Sci. Discuss.*, *17*, 627–639, doi:10.5194/nhess-2017-30.
- Kanamori, H. (1972), Mechanism of tsunami earthquakes, *Phys. Earth Planet. Inter.*, *6*, 346–359.
- Kelsey, H. M., et al. (1998), Paleoseismology of an active reverse fault in a forearc setting: The Poukawa fault zone, Hikurangi forearc, New Zealand, *Geol. Soc. Am. Bull.*, *110*, 1123–1148.
- Lay, T., Y. Yamazaki, C. J. Ammon, K. F. Cheung, and H. Kanamori (2011), The 2011 M_w 9.0 off the Pacific coast of Tohoku earthquake: Comparison of deep-water tsunami signals with finite-fault rupture model predictions, *Earth Planets Space*, *63*(7), 797–801, doi:10.5047/eps.2011.05.030.
- Li, L., K. F. Cheung, H. Yue, T. Lay, and Y. Bai (2016), Effects of dispersion in tsunami Green's functions and implications for joint inversion with seismic and geodetic data: A case study of the 2010 Mentawai M_w 7.8 earthquake, *Geophys. Res. Lett.*, *43*, 11,182–11,191, doi:10.1002/2016GL070970.
- Litchfield, N. J., et al. (2014), A model of active faulting in New Zealand, *N. Z. J. Geol. Geophys.*, *57*(1), 32–56, doi:10.1080/00288306.2013.854256.
- Litchfield, N. J., et al. (2016), 14th November 2016 M 7.8 Kaikoura earthquake. Preliminary surface fault displacement measurements, version 2, *GNS Sciences*, doi:10.21420/G2J01F.
- Mason, D. P. M., and T. A. Little (2006), Refined slip distribution and moment magnitude of the 1848 Marlborough earthquake, Awatere Fault, New Zealand, *New Zeal. J. Geol. Geophys.*, *49*(3), 375–382, doi:10.1080/00288306.2006.9515174.
- Nishenko, S. P., and W. R. McCann (1981), Seismic potential for the world's major plate boundaries: 1981, in *Earthquake Prediction: An International Review, Maurice Ewing Series*, pp. 20–28, AGU, Washington, D. C.
- Okada, Y. (1985), Surface deformation due to shear and tensile faults in a half space, *Bull. Seismol. Soc. Am.*, *75*(4), 1135–1154.
- Tanioka, Y., and K. Satake (1996), Tsunami generation by horizontal displacement of ocean bottom, *Geophys. Res. Lett.*, *23*, 861–864.
- Wallace, L. M., et al. (2007), Balancing the plate motion budget in the South Island, New Zealand using GPS, geological and seismological data, *Geophys. J. Int.*, *168*(1), 332–352.
- Wallace, L. M., et al. (2009), Characterizing the seismogenic zone of a major plate boundary subduction thrust: Hikurangi Margin, New Zealand, *Geochem. Geophys. Geosyst.*, *10*, Q10006, doi:10.1029/2009GC002610.
- Wallace, L. M., et al. (2012), The kinematics of a transition from subduction to strike-slip: An example from the central New Zealand plate boundary, *J. Geophys. Res.*, *117*, B02405, doi:10.1029/2011JB008640.
- Williams, C. A., et al. (2013), Revised interface geometry for the Hikurangi subduction zone, New Zealand, *Seismol. Res. Lett.*, *84*(6), 1066–1073.
- Yamazaki, Y., Z. Kowalik, and K. F. Cheung (2009), Depth-integrated, non-hydrostatic model for wave breaking and run-up, *Int. J. Numer. Methods Fluids*, *61*(5), 473–497.
- Yamazaki, Y., K. F. Cheung, and Z. Kowalik (2011a), Depth-integrated, non-hydrostatic model with grid nesting for tsunami generation, propagation, and run-up, *Int. J. Numer. Methods Fluids*, *67*(12), 2081–2107.
- Yamazaki, Y., T. Lay, K. F. Cheung, H. Yue, and H. Kanamori (2011b), Modeling near-field tsunami observations to improve finite-fault slip models for the 11 March 2011 Tohoku earthquake (M_w 9.0), *Geophys. Res. Lett.*, *38*, L00G15, doi:10.1029/2011GL049130.
- Yamazaki, Y., K. F. Cheung, and T. Lay (2013), Modeling of the 2011 Tohoku near-field tsunami from finite-fault inversion of seismic waves, *Bull. Seismol. Soc. Am.*, *103*, 1444–1455, doi:10.1785/0120120103.

Two regions of seafloor deformation generated the tsunami for the 13 November 2016, Kaikoura, New Zealand earthquake

Yefei Bai¹, Thorne Lay², Kwok Fai Cheung¹, and Lingling Ye³

¹Department of Ocean and Resources Engineering, University of Hawaii at Manoa, Honolulu, Hawaii, USA

²Department of Earth and Planetary Sciences, University of California Santa Cruz, Santa Cruz, California, USA

³Seismological Laboratory, California Institute of Technology, Pasadena, California, USA

Correspondence to: Kwok Fai Cheung, cheung@hawaii.edu

Contents of this file

Figure S1-S2

Animation M1

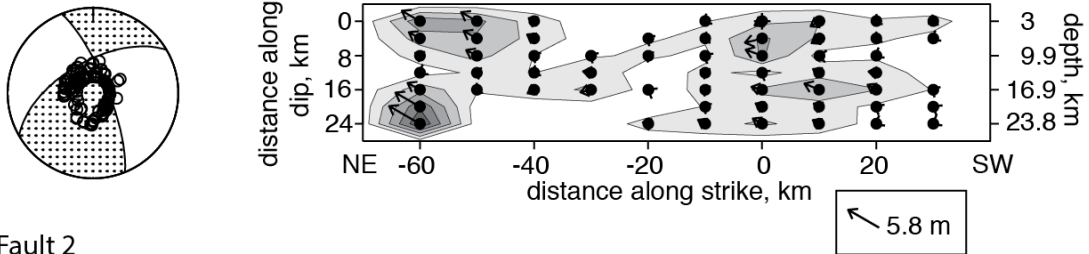
Introduction

Supporting information includes 2 figures and 1 animation.

Three-Fault Model
 Mo 7.27×10^{20} Nm, Mw 7.8

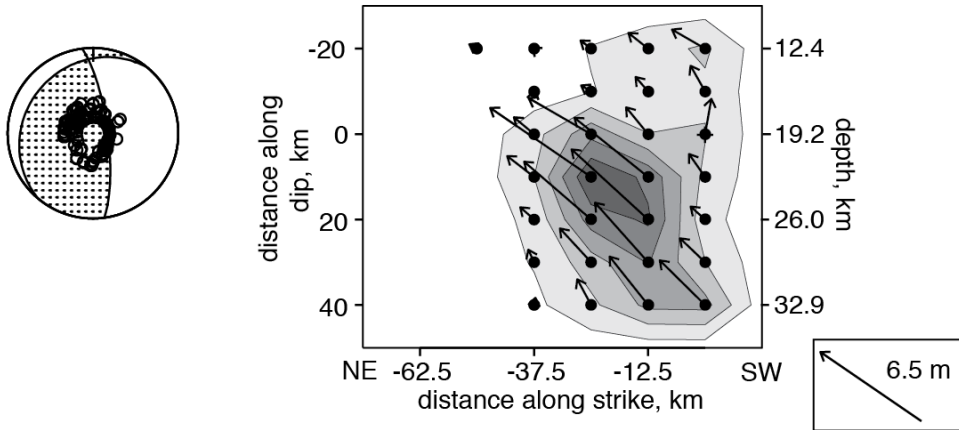
Fault 1

strike 240° , dip 60° , rake average 164°
 Vr 2.0 km/s, Mo 1.08×10^{20} Nm, start time 0 s



Fault 2

strike 220° , dip 20° , rake average 136°
 Vr 3.5 km/s, Mo 2.96×10^{20} Nm, start time 55 s



Fault 3

strike 232° , dip 60° , rake average 158°
 Vr 2.5 km/s, Mo 3.23×10^{20} Nm, start time 37 s

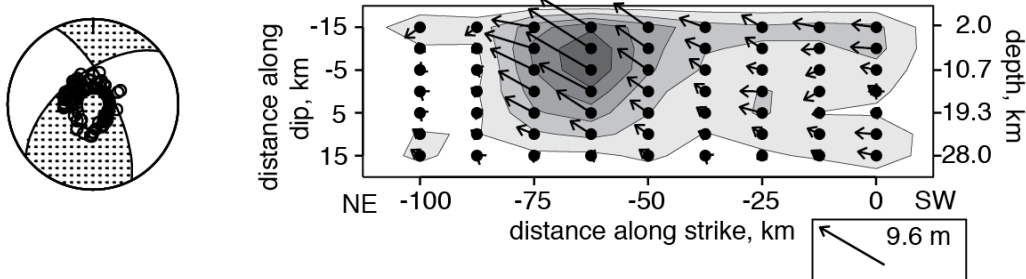


Figure S1. Final slip distribution on each fault in the three-fault model for the 2016 Kaikoura event. The faults are shown in relative spatial position in Figure 2. The strike, dip and rake of each fault are indicated along with a lower hemisphere projection showing the distribution of P waves used in the inversion. Actual *P* and *SH* observations and predicted ground motions for the model are shown in Figure S2. The vectors in the slip models indicate rake in the fault plane with lengths proportional to slip of the hanging wall (northwestern) side of the fault. The rupture expansion velocity, seismic moment, and initiation time of each fault are given.

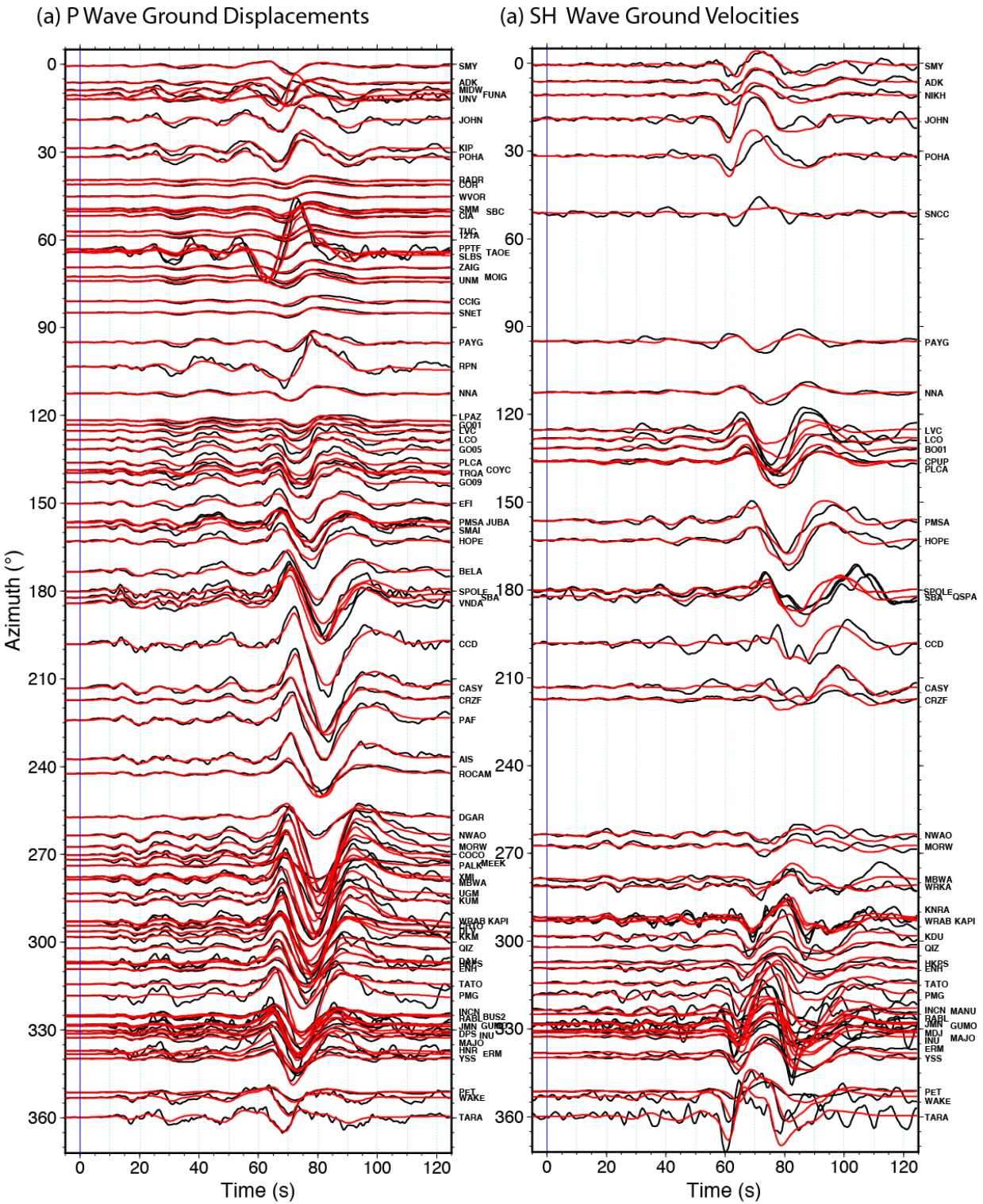
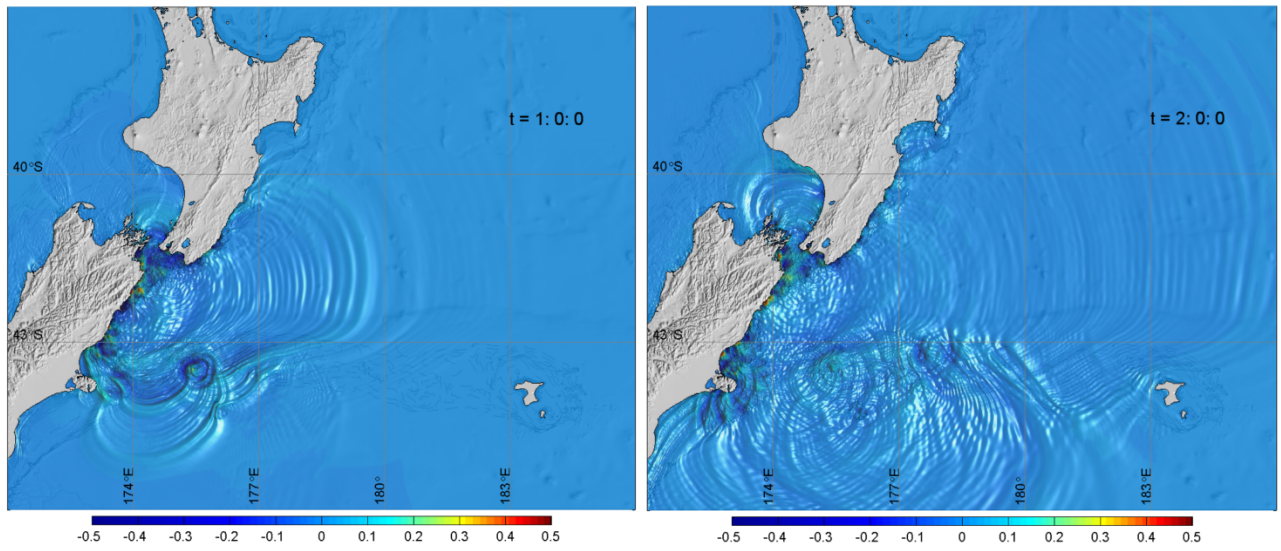


Figure S2. Comparison of observed (black lines) and computed (red lines) (a) *P*-wave ground displacements and (b) *SH*-wave ground velocity waveforms (right column) versus azimuth. The computed versions are for the preferred source model in Figure 2. The normalized residual waveform (difference of observed and predicted signals) power is 0.14, indicating 86% of the signal power is accounted for by the model.



Animation M1. The tsunami generated by the three-fault model of the 2016 Kaikoura, New Zealand earthquake.